A Highly-Accurate Industrial Robot Calibrator with Multi-Planer Constraints Supplementary Material

Tinghui Chen, Shuai Li, *Senior Member*, *IEEE*, Weiyi Yang, and Xin Luo, *Senior Member*, *IEEE*

This is the supplementary file for the paper, where the convergence proof of the AMPC algorithm is provided. Moreover, additional figures regarding partial experiments and results are placed here.

I. Convergence Analysis of AMPC

Given nodes $i \in m$, and iteration t, the convergence is divided into two sequential steps:
Step 1. The difference between Υ_{t+1} and Υ_t is bounded by that between (η_{t+1}, G_{t+1}, $a_{1,t+1}$) and (η_t, G_t, $a_{1,t}$);
Step 2. The augmented Lagrangian function (23) is non-increasing and low-bounded.

A. Proof of Step 1

This work provides proof with Γ as an active variable. Thus, *Lemma* 1 is presented as:

Lemma 1: With (29), $(\Upsilon_{t+1}-\Upsilon_t)^2$ is bounded by:

$$\left(\Upsilon_{t+1}-\Upsilon_t\right)^2 \le 2\left(\rho\left(\tau-1\right)\right)^2\left(\frac{1}{m}\sum_{i=1}^{m}\left(\Psi_i\left(a_{t+1},G_{t+1},\eta_{t+1}\right)-\Psi_i\left(a_t,G_t,\eta_t\right)\right)\right)^2+2\left(\frac{1}{m}\sum_{i=1}^{m}\left(\frac{1}{\kappa_{2,i,t+1}}\left(a_{1,t+1}+\kappa_{1,i,t+1}\right)-\frac{1}{\kappa_{2,i,t}}\left(a_{1,t}+\kappa_{1,i,t}\right)\right)\right)^2=v_{\Upsilon}, \tag{S1}$$

Proof: Consider that (23) is non-convex, implying that any equilibrium point having a zero-gradient (e.g., a saddle point or a global/local optimum) has the potential to be a feasible solution. Given the solution to a_1 by (29c) to be $a_{1,t+1}$, yielding:

$$\Upsilon_t+\frac{1}{m}\sum_{i=1}^{m}\left(\frac{1}{\kappa_{2,i,t+1}}\left(a_{1,t+1}+\kappa_{1,i,t+1}\right)+\rho\cdot\Psi\left(a_{t+1},G_{t+1},\eta_{t+1}\right)\right)=0, \tag{S2}$$

By replacing the values of Υ derived from equations (27d) and (29d) into expression (S2), we can derive:

$$\Upsilon_{t+1}=\left(\tau-1\right)\frac{\rho}{m}\sum_{i=1}^{m}\Psi_i\left(a_{1,t+1},G_{t+1},\eta_{t+1}\right)-\frac{1}{m}\sum_{i=1}^{m}\frac{1}{\kappa_{2,i,t+1}}\left(a_{1,t+1}+\kappa_{1,i,t+1}\right)=0, \tag{S3}$$

Hence, the difference between Υ_{t+1} and Υ_t is given as:

$$\Upsilon_{t+1}-\Upsilon_t=\left(\tau-1\right)\frac{\rho}{m}\sum_{i=1}^{m}\left(\Phi_i\left(a_{1,t+1},G_{t+1},\eta_{t+1}\right)-\Phi_i\left(a_{1,t},G_t,\eta_t\right)\right)-\frac{1}{m}\sum_{i=1}^{m}\left(\frac{1}{\kappa_{2,i,t+1}}\left(a_{1,t+1}+\kappa_{1,i,t+1}\right)-\frac{1}{\kappa_{2,i,t}}\left(a_{1,t}+\kappa_{1,i,t}\right)\right), \tag{S4}$$

With the inequality $(x\text{-}y)^2 \le 2(x^2+y^2)$, (S1) is fulfilled. Thus, *Lemma* 1 stands to implement Step 1.

B. Proof of Step 2

To facilitate the execution of Step 2, we present *Lemma* 2:

Lemma 2: If the following criteria are fulfilled, it is beneficial to define intermediate variables.

$$\rho\le 0,\ \tau\ge 0,\ \eta_{x,t}\ge 0,\ \eta_{y,t}\ge 0,\ \eta_{z,t}\ge 0, \tag{S5a}$$

$$\frac{1}{\kappa_{2,i,t+1}}\left(a_{1,t+1}+\kappa_{1,i,t+1}\right)\le 0,\ \tau\ge\frac{1}{2}, \tag{S5b}$$

Hence the following inequality is valid:

$$f\left(\eta_{t+1},G_{t+1},a_{1,t+1},\Upsilon_{t+1}\right)-f\left(\eta_t,G_t,a_{1,t},\Psi_t\right)\le 0, \tag{S6a}$$

$$f\left(\eta_{t+1},G_{t+1},a_{1,t+1},\Upsilon_{t+1}\right)\ge 0. \tag{S6b}$$

Proof: Considering the second-order Taylor expansion of f at the point of (γ_{t+1}, W_t, $a_{1,t}$ and Γ_t), we have:

$$f\left(\eta_{t+1},G_t,a_{1,t},\Upsilon_t\right)-f\left(\eta_t,G_t,a_{1,t},\Upsilon_t\right)\overset{(27a),(29a)}{=}\frac{\rho}{2m}\sum_{i=1}^{m}\begin{bmatrix}\kappa_{4,i,t}^2\left(\eta_{x,t+1}-\eta_{x,t}\right)^2+\kappa_{5,i,t}^2\left(\eta_{y,t+1}-\eta_{y,t}\right)^2\\+\kappa_{6,i,t}^2\left(\eta_{z,t+1}-\eta_{z,t}\right)^2\end{bmatrix}. \tag{S7}$$

Note that based on optimal conditions in (27a) and (29a), the first-order term is zero and has been omitted for brevity. Likewise, the difference between $f(\eta_{t+1}$, G_{t+1}, $a_{1,t}$ and $\Upsilon_t)$ and $f(\eta_{t+1}$, G_t, $a_{1,t}$ and $\Upsilon_t)$, and $f(\eta_{t+1}$, G_{t+1}, $a_{1,t+1}$ and $\Upsilon_t)$ and $f(\eta_{t+1}$, G_{t+1}, $a_{1,t}$ and $\Upsilon_t)$

can be formulated by:

$$f\left(\eta_{t+1},G_{t+1},a_{1,t},\Upsilon_t\right)-f\left(\eta_{t+1},G_t,a_{1,t},\Upsilon_t\right)\overset{(27b),(29b)}{=}\frac{\rho}{2m}\sum_{t=1}^{m}\left(\eta_{x,t+1}\left(G_{x,t+1}-G_{x,t}\right)^2+\eta_{y,t+1}\left(G_{y,t+1}-G_{y,t}\right)^2+\eta_{z,t+1}\left(G_{z,t+1}-G_{z,t}\right)^2\right) \quad \text{(S8)}$$

$$f\left(\eta_{t+1},G_{t+1},a_{1,t+1},\Upsilon_t\right)-f\left(\eta_{t+1},G_{t+1},a_{1,t},\Upsilon_t\right)\overset{(27c),(29c)}{=}\frac{1}{2m}\sum_{i=1}^{m}\left(1+\rho\kappa_{2,i,t}^2\right)\left(a_{1,t+1}-a_{1,t}\right)^2. \quad \text{(S9)}$$

Additionally, $f(\eta_{t+1}, G_{t+1}, a_{1,t+1}$ and $\Upsilon_{t+1})$ and $f(\eta_{t+1}, G_{t+1}, a_{1,t+1}$ and $\Upsilon_t)$ are differed as:

$$f\left(\eta_t,G_{t+1},a_{1,t+1},\Upsilon_{t+1}\right)-f\left(\eta_t,G_t,a_{1,t},\Upsilon_t\right)\overset{(27d),(29d)}{=}\frac{\left(\Upsilon_{t+1}-\Upsilon_t\right)^2}{\tau\rho}\overset{S1}{\leq}\frac{v_\Upsilon}{\tau\rho}. \quad \text{(S10)}$$

With (S9), the equality can be deduced from the update rules (27d) and (29d), whereas the inequality is contingent upon the premises established in Lemma 1. Through a logical combination of equations (S7) to (S10), the following result can be inferred:

$$\begin{aligned}
&f\left(\eta_t,G_{t+1},a_{1,t+1},\Upsilon_{t+1}\right)-f\left(\eta_t,G_t,a_{1,t},\Upsilon_t\right)\leq\frac{\rho}{2m}\sum_{i=1}^{m}\left(\kappa_{4,i,t}^2\left(\eta_{x,t+1}-\eta_{x,t}\right)^2+\kappa_{5,i,t}^2\left(\eta_{y,t+1}-\eta_{y,t}\right)^2+\kappa_{6,i,t}^2\left(\eta_{z,t+1}-\eta_{z,t}\right)^2\right)\\
&+\frac{\rho}{2m}\sum_{i=1}^{m}\left(\eta_{x,t}\left(G_{x,t+1}-G_{x,t}\right)^2+\eta_{y,t}\left(G_{y,t+1}-G_{y,t}\right)^2+\eta_{z,t}\left(G_{z,t+1}-G_{z,t}\right)^2\right)^2+\frac{1}{2m}\sum_{i=1}^{m}\left(1+\rho\kappa_{2,i,t}^2\right)\left(a_{1,t+1}-a_{1,t}\right)^2\\
&+\frac{2}{\tau}(\tau-1)^2\rho\frac{1}{m}\sum_{i=1}^{m}\left(\Phi_i\left(a_{t+1},G_{t+1},\eta_{t+1}\right)-\Phi_i\left(a_t,G_t,\eta_t\right)\right)^2+2\frac{1}{\rho\tau}\left(\frac{1}{m}\sum_{i=1}^{m}\left(\frac{1}{\kappa_{2,i,t+1}}\left(a_{1,t+1}+\kappa_{1,i,t+1}\right)-\frac{1}{\kappa_{2,i,t}}\left(a_{1,t}+\kappa_{1,i,t}\right)\right)\right)^2\leq 0, \quad \text{(S11)}\\
&\Rightarrow\rho\leq 0,\eta_{x,t}\geq 0,\eta_{y,t}\geq 0,\eta_{z,t}\geq 0,\frac{2}{\tau}(\tau-1)^2\rho\leq 0,\frac{1}{\rho\tau}\leq 0,\\
&\Rightarrow\rho\leq 0,\eta_{x,t}\geq 0,\eta_{y,t}\geq 0,\eta_{z,t}\geq 0,\tau\geq 0.
\end{aligned}$$

Hence, (S5a) and (S6a) are fulfilled, which demonstrates that (23) is non-increasing in this case. After (*t*+1)-*th* iteration, (23) can be reformulated as:

$$f\left(\eta_{t+1},G_{t+1},a_{1,t+1},\Upsilon_{t+1}\right)=\frac{1}{2m}\sum_{i=1}^{m}\left\|B_i-\hat{C}_i\right\|_2^2+\frac{1}{m}\sum_{i=1}^{m}\left\langle\Psi_i\left(a_{1,t+1},G_{t+1},\eta_{t+1}\right),\Upsilon_{t+1}\right\rangle+\frac{1}{2m}\sum_{i=1}^{m}\rho\left\|\Psi_i\left(a_{1,t+1},G_{t+1},\eta_{t+1}\right)\right\|_2^2, \quad \text{(S12)}$$

By substituting (S3) into (S11), we can obtain:

$$f\left(\eta_{t+1},G_{t+1},a_{1,t+1},\Upsilon_{t+1}\right)=\frac{1}{2m}\sum_{i=1}^{m}\left\|B_i-\hat{C}_i\right\|_2^2+\frac{(2\tau-1)\rho}{2}\frac{1}{m}\sum_{i=1}^{m}\left(\Phi_i\left(a_{1,t+1},G_{t+1},\eta_{t+1}\right)\right)^2-\frac{1}{m}\sum_{i=1}^{m}\frac{1}{\kappa_{2,i,t+1}}\left(a_{1,t+1}+\kappa_{1,i,t+1}\right), \quad \text{(S13)}$$

with (S5b) and (S13), (S6b) is fulfilled, i.e., (23) is lower-bounded. Hence, *Lamma* 2 stands, making Step 2 complete. To sum up, as per the aforementioned deductions, with the implementation of Steps 1 through 2, AMPC's convergence can be established with certainty in theory.

II. Additional Figures

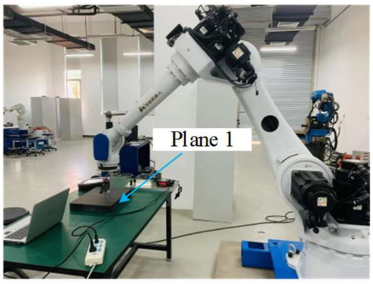

(a)

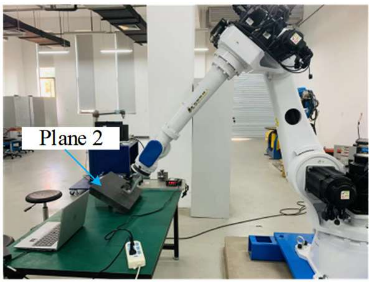

(b)

(c)

Fig. S.1. The samples collection process on D1-3. (a), (b) and (c) are corresponded to D1-3, respectively.

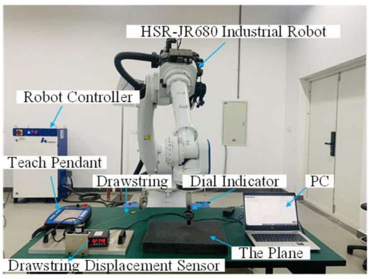

(a)

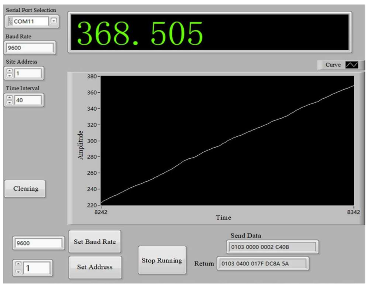

(b)

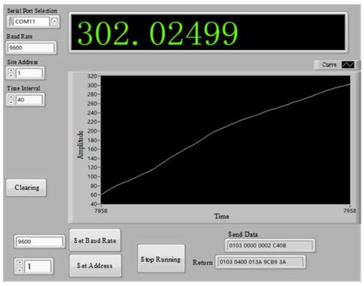

(c)

Fig. S.2. The experimental system. (a) The experimental platform, (b) and (c) The LabVIEW software on two different samples.

(a)

(b)

(c)

Fig. S.3. The experimental process. (a), (b) and (c) depict three various measurement positions on D1.

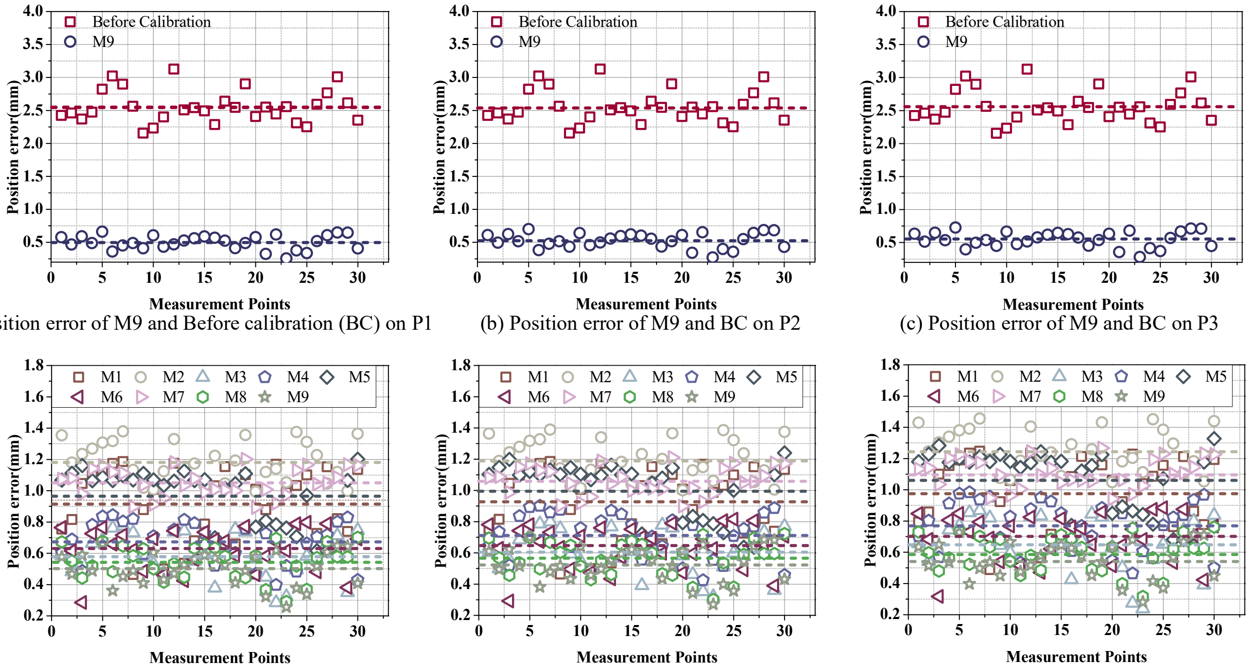

(a) Position error of M9 and Before calibration (BC) on P1
(b) Position error of M9 and BC on P2
(c) Position error of M9 and BC on P3
(d) Position error of M1-9 on P1
(e) Position error of M1-9 on P2
(f) Position error of M1-9 on P3

Fig. S.4. The position error of the industrial robot after calibration using various algorithms on P1-3. Note that the dotted lines represent the average values. Panels (a)-(c) illustrate that the industrial robot obtains an evident enhancement of position accuracy after calibration. Panels (d)-(f) show that M9 has the best position accuracy when compared to M1-8.